A feasible method of support slimming based on the different thresholds of polar angles in selective laser melting

Kaifei Zhang[a]

Zhongfa Mao[a]

Guang Fu[a]

David Z. Zhang[a, b, *]

zhangzw@cqu.edu.cn

Chao Liu[a]

Zhonghua Li[c]

[a]State Key Laboratory of Mechanical Transmissions, Chongqing University, 400044, Chongqing, China

[b]College of Engineering, Mathematics and Physical Sciences, University of Exeter, North Park Road, Exeter EX4 4QF, UK

[c]School of Mechanical Engineering, North University of China, 030051, Taiyuan, Shanxi Province, China

[*]Corresponding author at: State Key Laboratory of Mechanical Transmissions, Chongqing University, 400044, Chongqing, China.

Abstract

The large thermal deformation induced by the high temperature gradient severely restricts the threshold level of polar angle in selective laser melting (SLM). As such, different types of support structures are usually added to improve the manufacturing capacity and broaden the application of SLM technology. However, enormous support structures will result in large time consumption, material waste, high labor intensity and inferior surface quality of part. In this research, a feasible method of slimming support structures was presented. Firstly, a series of experiments for exploring the thresholds of polar angles at different azimuth angles relative to the recoating direction of powders were conducted and the effect of powder recoating by scraper on the building of inclined surfaces was analyzed. Then, a generation algorithm of slimmed support structures was proposed based on the varying thresholds of polar angles. In addition, several typical cases demonstrated the usefulness of this method by eliminating the quantities of their support structures by 35 percent% in average.

Keywords: Selective laser melting; Threshold; Polar angle; Azimuth angle; Support slimming

1. Introduction

Selective laser melting (SLM) is widely regarded as one of the most promising additive manufacturing (AM) technologies, which enables the quick production of complex-shaped and compact three-dimensional (3D) parts directly from metal powder [1, 2]. SLM technology uses laser as the energy source to melt metal powders layer-by-layer according to the two-dimensional (2D) slice profile of part under the protection of inert gases such as nitrogen and argon, which is suitable for all types of materials in theory [3].

In SLM, there are still some defects such as staircase effect and thermal distortion. Staircase effect usually occurs in the case of manufacturing inclined surfaces including both upper surfaces and downward surfaces. Due to the stepped approximation by layers of curved and inclined surfaces, the staircase effect affects the surface roughness through altering the layer thickness and the polar angle of surface [4]. When building a part in SLM, a small layer thickness can effectively reduce the surface roughness but greatly increase the building time [4–6]. When the polar angle of the inclined surface is reduced, it is more pronounced to deteriorate the surface roughness [7]. In order to minimize the staircase effect, multi-axis processing method in which the slicing direction rotates to 90°, in case of an overhang structure instead of taking the classical parallel slicing procedure was presented [8, 9]. Moreover, the rapid melting and solidification of powders in SLM process results in a nonuniform temperature distribution, which causes large thermal stresses within solidified part [10]. With it comes a poor property such as large distortion of part, or more seriously, an interruption of the processing process. In order to reduce the deformation of the fabricated part, Mohanty and Hattel [11] analyzed the effect of several different types of scanning strategies on the temperature

distribution through simulation. Chen et al. [12] improved the AM processability of the hard-to-process overhanging structure by selecting an optimal laser volume energy density obtained through optimizing the processing parameters. In addition, to control the thermal deformation induced by the temperature gradient, increasing the preheating temperature, controlling building chamber temperature and using intermediary powder blends were also proposed as effective methods of reducing deformation of fabricated parts [13–15]. However, some inclined surfaces with too small inclination angles will still not be able to be processed without any other auxiliary structures because of the existence of the large residual stress and distortion. In another word, there is a limit to the inclination of a manufacturable downward surface without help of auxiliary structures. Based on this processing limit, some researchers have presented a number of new design methods for industrial components which are better suited for manufacturing via SLM [16–18].

To resist the distortion induced by the large temperature gradient, support structures are also usually added to help to form complicated parts with lots of inclined surfaces in SLM. Järvinen et al. [19] described several types of conventional support structures, such as block support, point support, web support, contour support and line support, which were widely used in SLM. In addition, some design methods of new support structures were developed in [20–23]. However, enormous support structures would result in large time consumption, material waste, labor intensity and inferior surface quality of parts. Mumtaz et al. [24] presented a special method of eliminating support structures by applying selective laser sintering (SLS) material principles to SLM. Unfortunately, the application scope of this method is too narrow up to now. Jhabvala et al. [25] used a pulsed laser to build support structures to increase the building efficiency and reduce the labor intensity because this laser could make quicker scanning speed and structures with higher porosity. Calignano [7] optimized the supports by using a statistic method to analyze the significance of the structure parameters of supports. Krol et al. [26] obtained the optimal support structures by simulations before manufacturing to ensure the success rate and decrease the material waste. Kuo et al. [27] used a topology optimization method to slim the supports while Morgan et al. [28] cut the quantity of support structures by optimizing the part orientation.

Although a large number of researches about the manufacturing feasibility of inclined surfaces, especially downward surfaces, have been reported, they almost neglected another factor: the tool with function of spreading powders built as a scraper or a roller that is an essential part of SLM machine. This tool influences not only the property of the powder bed but also the processing of parts, especially for the downward surfaces. Although Pham and Ji [29] and some other researchers have dedicated efforts to optimize the control or the design of the scraper or roller, there is still limit in getting insight of the effect of the tool on the fabrication of inclined surfaces. In fact, the existence of this tool will result in an anisotropy of inclined-surface manufacturability in SLM, that is to say, the threshold of the polar angle is different at different directions with respect to the recoating direction. At present, as what mentioned before, most researchers mainly focus on either optimizing the support structures based on a constant polar angle threshold or designing new types of support structures directly. Therefore, this study is aimed at analyzing the effect of scraper on the fabrication of downward surfaces, and then based on the effect developing an original building algorithm of optimized supports in SLM. In addition, the feasibility of this algorithm for reducing the forming supports of the parts ~~are~~is further validated.

~~2.~~2 Method

Most of common support generation softwares, e.g. Magics 20.03 (Materialise, Belgium), usually generate support structures according to a settable constant polar angle. In comparison, an original and feasible method of minimizing support structures, which is based on the varying polar angle thresholds obtained by experiments is given out in the following.

~~2.1.~~2.1 Thresholds of polar angles

As known to all, the threshold of polar angle changes with the different material and its different processing parameters in SLM. Titanium alloy (Ti-6Al-4V) with high specific strength and good biocompatibility is widely used in the areas of aerospace, motor industry and medical treatment. As such, Ti-6Al-4V is chosen to explore the thresholds of polar angles under a series of processing parameters in this research.

~~2.1.1.~~2.1.1 *Experimental method*

Experiments were performed on the commercial SLM machine EOSINT M280 (EOS GmbH, Krailling, German) equipped with a single-mode continuous wave ytterbium fiber laser YLR-200 (IPG Photonics, Oxford, MS, USA) operating at a wavelength of 1.07 μm and producing a laser beam with an energy intensity distribution with a Gaussian profile. The feedstock material used for this investigation was gas-atomized Ti-6Al-4V powder (EOS art.-no.9011-0014, EOS GmbH, Krailling, German) with a chemical composition corresponding to the standards (ISO 5832-3, ASTM F1472 and ASTM B348), as listed in Table 1 in detail. The processing parameters were also summarized in Table 2 particularly. The same laser power and scanning speed were used to form both core and contours of part and the cross-hatching scanning strategy was employed whereby parallel alternative scan vectors were overlaid at an angle of 67° to the previous deposited layer. In this investigation, the scraper moving from the feed region to the overflow region to form a new powder bed was made from high-speed steel (HSS). After a deposited layer was completed, the build platform arranged in the middle of the feed region and the overflow region would move down for a distance of 1 mm (quite larger than the layer thickness) to avoid the contact between the powder bed and the scraper. Then the scraper moves back quickly from the overflow region to the feed region. After that, the build platform moves up for 0.97 mm to achieve the specified layer thickness and the scraper spreads powders from the feed region to form a new powder bed repeatedly.

Table 1 Chemical compositions of EOS Titanium alloy Ti-6Al-4V powder.

alt-text: Table 1

Elements	Ti	Al	V	O	N	C	H	Fe
Content (wt.%)	Balance	5.5–6.75	3.5–4.5	<0.2	<0.05	<0.08	<0.015	<0.3

Table 2 SLM process parameters of EOS Titanium alloyTi-6Al-4V powders.

alt-text: Table 2

Process parameter	Value
Laser power	170 W
Spot diameter	100 µm
Scanning speed	1250 mm/s
Hatch distance	100 µm
Layer thickness	30 µm
Atmosphere	Ar (Oxygen level < 0.1%)
Preheating temperature	35 °C

The specimens for investigating the polar angle thresholds were designed as a series of heptahedrons that could be divided into cuboids and quadrangular prisms, as depicted in Fig. 1. The cuboids of all specimens are same with 3 mm length, 3 mm width and 1 mm height, but the quadrangular prisms are different in vertical sections of right trapezoid in spite of their same thickness of 3 mm. The heights of the prism vertical sections are same of 10 mm and the lengths of bottom side are constant 3 mm that is equal to the thickness of prisms, while the inclination angles of the sloping sides are different. In Fig. 1, $\boldsymbol{I}_n$ is the normal vector of the downward inclined surface of the specimen, $\boldsymbol{I}_{np}$ is the projection of $\boldsymbol{I}_n$ in the build platform and $\boldsymbol{I}_{rec}$ is the recoating direction. The azimuth angle between $\boldsymbol{I}_{rec}$ and $\boldsymbol{I}_{np}$, i.e. α, changes by 45° from 0° to 315°. $\boldsymbol{N}_{ob}$ is a unit vector opposite $\boldsymbol{I}_{acc}$ which is the building direction. The polar angle (γ) between $\boldsymbol{I}_n$ and $\boldsymbol{N}_{ob}$ expressing the inclination of specimen changes by 5° from 15° to 40° for primary investigation and then by 1° for detail investigation to decrease the amount of experiments. In order to obtain the accurate threshold of the polar angle, i.e. γ_{lim}, a weak block support structure (Fig. 2) was applied to support the bottom surface of each specimen. If a specimen lost resolution in its sharp corner or was swept away from its support structure by the scraper or the recoating process of powder bed was interrupted due to the warpage of specimen, this polar angle of the specimen would be regarded as unshaped or undesirable angle. In other words, only when the specimen was manufactured well and completely, this polar angle of the specimen could be treated as a desirable angle. Then the minimum of the desirable angles is the threshold of the polar angle.

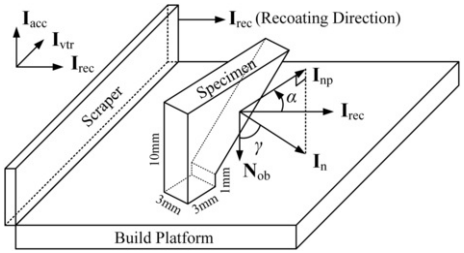

Fig. 1 Map of specimens used in experiments.

alt-text: Fig. 1

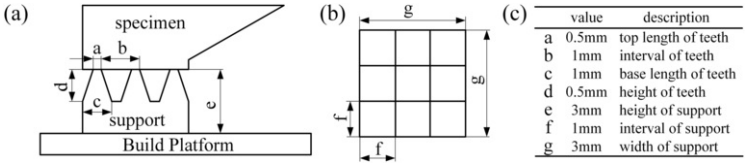

Fig. 2 (a) Weak support structure under the bottom surface of specimen and (b) corresponding projection in the build platform as well as (c) parameters of support.

alt-text: Fig. 2

~~2.1.2.~~2.1.2 Results and discussion

According to the design of experiment, the experimental results are listed in ~~table~~Table 3 where the results in primary investigation with change of α by 5° are marked in black and those in detail investigation with change of α by 1° are marked in red. If the specimen could be successfully fabricated, marking it as "√", otherwise marking it as "×".

Table 3 Total results of the formation of the inclined surfaces.

alt-text: Table 3

	γ																	
α	15°	20°	21°	22°	23°	24°	25°	26°	27°	28°	29°	30°	31°	32°	33°	34°	35°	40°
0°	×	×	×	×	×	√	√					√					√	√
45°	×	×					×	√	√	√	√	√					√	√
90°	×	×					×	×	×	×	√	√					√	√
135°	×	×					×					×	√	√	√	√	√	√
180°	×	×					×					×	×	√	√	√	√	√
225°	×	×					×					×	√	√	√	√	√	√
270°	×	×					×	×	×	×	√	√					√	√
315°	×	×					×	√	√	√	√	√					√	√

During primary investigation, it can be seen from ~~table~~Table 3 that the threshold of the polar angle (γ_{lim}) increases as the α (0°~180°) increases, suggesting that the better forming property is, the smaller α is. Furthermore, the relatively accurate γ_{lim} has been obtained in detail investigation. Based on the obtained experimental datum, a fitting curve can be drawn as shown in Fig. 3, expressing the relationship between the γ_{lim} and the α. It can be found that this curve is axisymmetric on α=180°, thus the directional change between $\boldsymbol{I}_{rec}$ and $\boldsymbol{I}_{np}$ will be neglected in following text. A governing equation of γ_{lim} and α can be acquired and expressed as Eq~~uation~~. (1).

$$g_{lim} = \gamma(\alpha)\ (\alpha = 0° \text{-} 180°) \quad (1)$$

(Eq. 1 needs to be modified. The first letter "g" needs to be changed by Greek letter gama. Please refer to the attachment.)

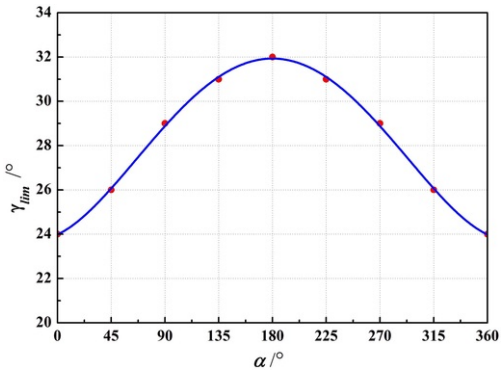

Fig. 3 Fitting curve expressing the relationship between γ_{lim} and α.

alt-text: Fig. 3

In order to understand better the effect of α on γ_{lim}, the specimens with different polar angles at α of 0° and 180° are shown in Figs. 4–5. Thanks to the different degree of thermal deformation in the sharp corners caused by γ and α, the different

final forming heights of the specimens can be clearly seen, indicating that the building difficulties of these specimens increase with the decrease of γ and the sharp corner will own a higher resolution when the γ increase. For a given layer thickness, the overhang length (Fig. 6a) obtained by comparing two adjacent layer slices increases as the inclination angle decreases from γ_1 to γ_2. Because there is no constraint under the overhang, a longer overhang length will cause a larger deformation and the deformation magnitude continues to increase along the building direction [30]. In this case, a flatter inclined surface will be harder to be fabricated. On the other hand, for a given polar angle, the overhang length increases with the increase of layer thickness, which will result in the same influence on the deformation as the decrease of polar angle. Due to the layer thickness has significant influence on the stability of molten pool, which will tend to reduce the surface tension, easily leading to balling effect and deterioration in surface roughness [31]. Therefore, the layer thickness should theoretically be as thin as possible. In this work, layer thickness was set to 30 μm, which was decided by the powder particle size (the mean particle diameter is about 30 μm).

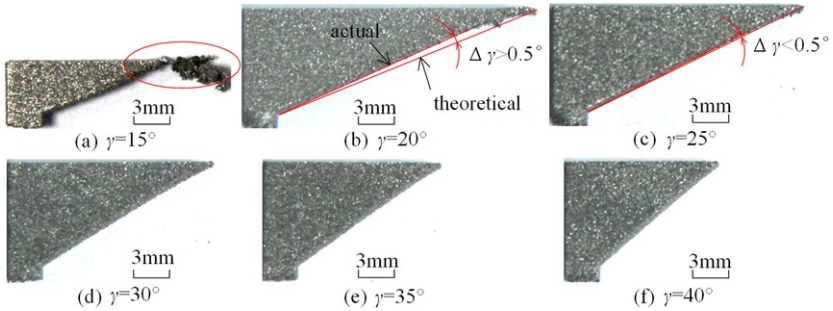

Fig. 4 Specimens with different inclination angles formed at $\alpha = 0°$.

alt-text: Fig. 4

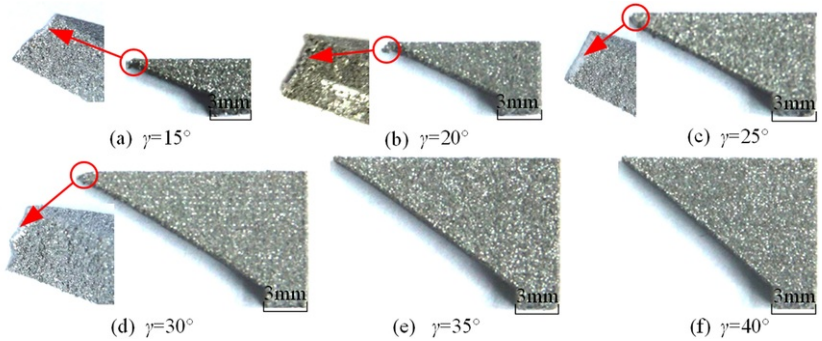

Fig. 5 Specimens with different inclination angles formed at $\alpha = 180°$.

alt-text: Fig. 5

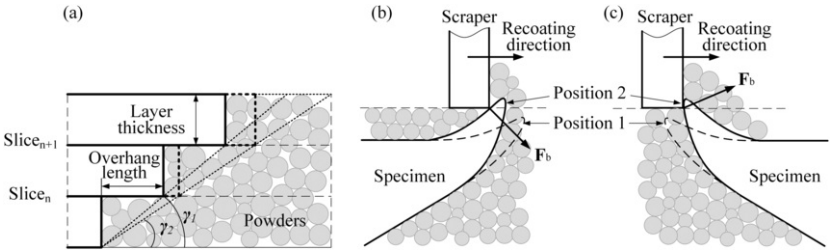

Fig. 6 The schematics of (a) the change of overhang length with γ and the recoating process in SLM (b) at $\alpha = 0°$ and (c) at $\alpha = 180°$.

alt-text: Fig. 6

Furthermore, comparing the specimens at α=0° (Fig. 4) with those at α=180° (Fig. 5), a major difference can be found in the distortional morphologies of the sharp corners and final forming heights of the specimens. For α= 0°, the sharp corner curves upward to be broken finally (Fig. 4a) or forms a long tip resulting in a lost in its resolution (Fig. 4b). As shown in Fig. 4b, two lines are drawn to express the actual and theoretical downward surfaces. One is created from the bottom of the inclined surface along its actual border. The other is created through the bottom of the inclined surface and the vertex of its sharp corner. If the angle between the two lines is larger than half of the minimum variation of designed polar angles, i.e. $\Delta\gamma$>0.5°, the resolution of the sharp corner is considered to be lost. Conversely, the precision of the inclined surface is considered to be accepted, such as the angle in Fig. 4c. However, for α=180°, it is worthy noted that the distortion and tip of the sharp corners are invisible and these have been replaced by some fracture morphologies (Fig. 5(a–d)), which is attributed to the impact of scraper on the deformed sharp corners. The resultant difference above at different α can be elucidated by the schematic of the recoating process in SLM (Figs. 6(b, c)). In Fig. 6(b), when the part with an polar angle (γ) is built at α=0°, the possible thermal distortion (position 1) occurs in the sharp corner and it will become worse (position 2) with the increase of the building height in SLM due to the accumulation of thermal stress [32]. It is therefore that the sharp corner will be affected by a force ($\mathbf{F}_b$) pointing the bottom right, which is in favor of the suppression of the buckling deformation in some extent. This also further explains the experimental results in Fig. 4 that the parts with the α beyond 25° can be successfully fabricated. However, it is different from the specimens at α=0° that the specimens at α=180° will be affected by a force ($\mathbf{F}_b$) pointing upper right (Fig. 6(c)) which has a facilitation effect on the buckling deformation, resulting in the crash of the sharp corner and the interruption of forming process in SLM. This is consistent with the experimental results in Fig. 5 that these parts can be successfully fabricated only when the α beyond 35°. Therefore, it can be concluded that the influence of α on forming deformation in the sharp corner can be divided into two categories containing suppression effect and facilitation effect. In addition, the significance of the effects of different α on forming property are further discussed in Figs. 7 and Fig. 9. Here, the polar angles (γ) are fixed at a small value of 25° and at a relative major value of 40° respectively, and the α is treated as a variable.

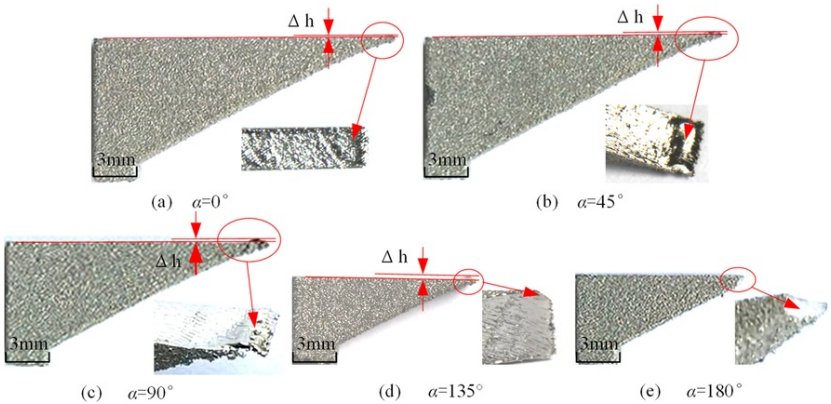

Fig. 7 Specimens with the same γ of 25°, created at different angles of α.

alt-text: Fig. 7

Fig. 7 shows the specimens with the same γ of 25° and different α. It can be clearly seen that the warpage levels expressed by Δh of the parts at different α are diverse. Moreover, the trend in ~~table~~Table 3 that the forming properties of the parts become more superior as the α increases has been obtained. These experimental results can be explained by a schematic diagram in Fig. 8. For the same γ, the distortions of all the specimens can be assumed to be uniform and form a contact area of a contact width (D_w) with the scraper. The contact length (CL) between the scraper and the specimen is directly affected by α value and expressed as Eq~~uation.~~ (2). Thus, combined Fig. 6 with Fig. 8, it can be inferred that the significance of effects of α on the forming property is determined by CL value. During the range of the α (0°-90°), CL value decreases with the increase of the α, indicating that the suppression effect of scraper on the deformation in the sharp corner is gradually weakened and tended to eliminate. However, it is interesting that the facilitation effect of scraper on the deformation in the sharp corner is gradually strengthened when the α increases form 90° to 180° based on the Eq~~uation.~~ (2). In general, these different effects caused by different α contribute the different forming property of the specimens in SLM.

$$CL = D_w \cdot \cos\alpha \quad \textbf{(2)}$$

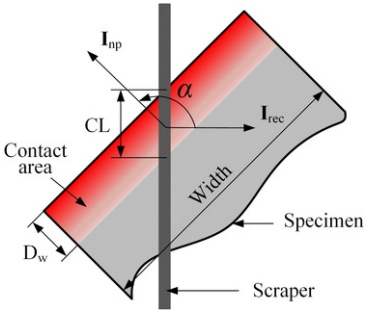

Fig. 8 Map of the change of the contact length with α.

alt-text: Fig. 8

For the γ of 40°, there are no clear distinctions among the sharp corners of the specimens built at different position of α, as depicted in Fig. 9. All the specimens can be successfully fabricated and present high-quality sharp corners. This can be clarified by that the formation would not be impacted by the scraper when the warpage of a specimen is too small to exceed the bottom of the scraper.

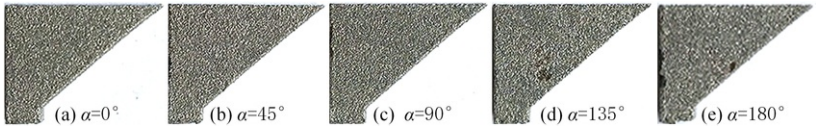

Fig. 9 Specimens with the same γ of 40° and created at different angles of α.

alt-text: Fig. 9

According to Fig. 3, the specimens with polar angle of 20° at azimuth angles of 0° need to be supported for precise shapes in processing while those with polar angle of 25° do not require additional support structures. However, they should all be supported by conventional method because their polar angles are smaller than the maximum of γ_{lim}. For comparison, two types of support structures were added to create the specimens at azimuth angles of 0° as shown in Fig. 10. It can be clearly seen that the precision of the specimens in Fig. 10a and ~~Fig. 10~~c are highly increased compared with that of the specimen in Fig. 4b. Simultaneously, support structures influence the microstructure development during SLM. Due to the faster heat conduction by support structures, finer grains develop in the boundary regions separating the specimen and the support structure while the crystallographic texture development in the core part of the specimens is mostly independent of the support configuration [33]. The support B (Fig. 10) increases the cooling rate of the downward surfaces leading to a raise in the thermal stress but its connection with specimen resists the large thermal stress to improve the precision. However, distortions (Figs. 10a–b) have appeared because the support A is much weaker than the support B. The specimens (Fig. 10c and ~~Fig. 10~~d) formed directly from the build platform without support A are in good precision. Although the precision of the specimens in Fig. 10b and ~~Fig. 10~~d is slightly higher than that of the specimen in Fig. 4c, the time consumption, the material waste and the labor intensity both become greater and the downward surfaces will become rougher after removing the support structures. Therefore, it is worthy to reduce the unnecessary support structures especially in processing the complex metal parts without strong request on precision.

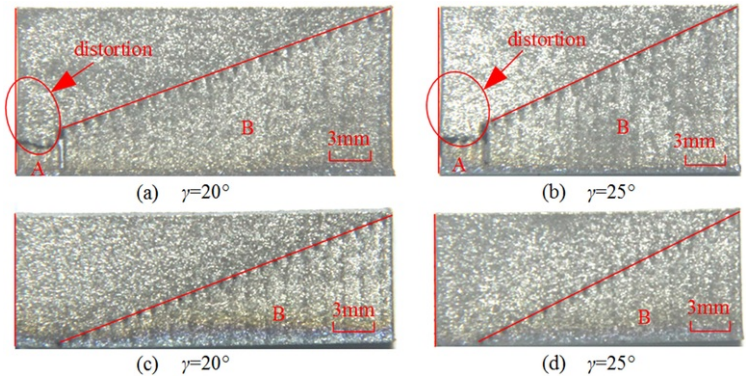

Fig. 10 Specimens with different support structures, created at α of 0°.

alt-text: Fig. 10

~~2.2.~~2.2 Slimmed-support generation algorithm

It is essential to minimize the use of supports as reduced contact area between the part and these structures will result in better part quality and also reduce the post processing efforts [34]. As discussed before, the thresholds of polar angles change with the azimuth angle. That is to say, we need to consider different polar angle thresholds instead of constant polar angle threshold in all directions as common when we create supports to prevent distortions. Therefore, an original slimmed-support generation algorithm expressed by a flow chart (Fig. 11) was developed considering the anisotropy of inclined-surface manufacturability [35].

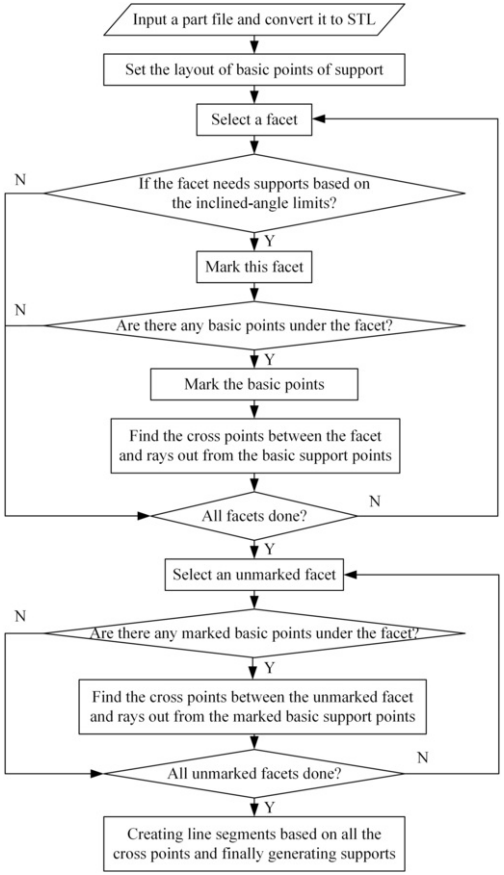

Fig. 11 The flow chart of the slimmed-support generation algorithm.

alt-text: Fig. 11

In the additive manufacturing industry, STL format is a standard and common file type that uses triangular facets consisting of their normal vectors and three vertex coordinates to express three-dimensional parts. After converting original part file to STL file, the bounding box of part could be easily obtained by comparing all coordinates of the vertexes of facets. Then a layout of basic support points, such as the separation distance of every two basic support points, needs to be made in the horizontal plane (Fig. 12a). A more accurate method of setting the basic points layout can be applied according to another research [36]. Next, a single triangular facet is selected to be distinguished whether requiring supports or not by:

$$Req = \begin{cases} 1, \gamma < \gamma_{\lim} \\ 0, \gamma \geq \gamma_{\lim} \end{cases} \quad (3)$$

where γ is defined as

$$\cos\gamma = \frac{I_{nf} N_{ob}}{\left| I_{nf} \right|} \quad (4)$$

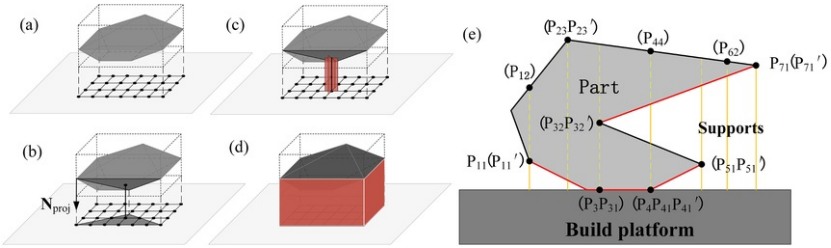

Fig. 12 The process of generating the support: (a) set the layout of basic points of the support; (b) find the cross point of the facet and a ray; (c) create a single cross-shaped support piece; (d) create the final support; (e) deal with the special points.

alt-text: Fig. 12

In Equation (3), $\boldsymbol{I}_{nf}$ is the normal vector of the selected facet and $\boldsymbol{N}_{ob}$ is the unit vector opposite the building direction. According to the experimental results and Equation (1), it was indicated that γ_{lim} is not a constant but a variable related to the value of α which can be obtained through:

$$\cos\alpha = \frac{\left(\left(N_{ob} \times I_{nf} \right) \times N_{ob} \right) \cdot N_{rec}}{\left| \left(N_{ob} \times I_{nf} \right) \times N_{ob} \right|} \quad (5)$$

where $\boldsymbol{N}_{rec}$ is an unit vector along the recoating direction. Actually, for a higher success rate of completing a part, we can adjust Equation (1) into:

$$\gamma_{lim} = \gamma(\alpha) + \gamma_s \ (\alpha = 0° \sim 180°) \quad (6)$$

where γ_s is an addition for safety. Here, attentions should be paid to the fact that the γ_{lim} should be acquired by experiments under the specified material and process parameters. If the used powder material and its process parameters are different from those in this investigation, the value of γ_{lim} and the Equation (6) need to be accordingly modified [37].

If the value of *Req* is 0, there's no need to support this triangular facet and another single triangular facet can be done as before. Otherwise, we need to mark this facet and check if there are any basic support points in the projection area of this facet in the horizontal plane. The projection vector is $\boldsymbol{N}_{proj}$ (Fig. 12b). If the layout of basic support points is too sparse, some small facets may have no basic support points under them. They will wherefore have no need to be supported although theoretically needing supports due to their small polar angles according Equation (3). When there are some basic support points in the facet projection, we need to mark these basic support points. Then we can create a series of support rays from these points along $\boldsymbol{N}_{proj}$ and then calculate the ordinates of the cross points between these rays and the facet (Fig. 12b) according to the following steps:

a. Calculate the coordinates of the projection points of the facet's three vertexes along $\boldsymbol{N}_{proj} = (x_{proj}, y_{proj}, z_{proj})$ in the horizontal plane. We express the three facet vertexes by $P_i(x_i, y_i, z_i)$ (i=1,2,3) and the projection points in the horizontal plane of the three facet vertexes by $P_i'(x_i', y_i', 0)$ (i=1,2,3) respectively. Then we can get $x_i' = x_i - z_i x_{proj}/z_{proj}$ and $y_i' = y_i - z_i y_{proj}/z_{proj}$ easily.

b. Determine whether the selected basic support point locates in the facet projection. We assume $\Omega(f)$ is the projection area in the horizontal plane of a facet whose three sides are not included and $\Omega(s)$ is the projection segments of this facet's three sides. Then we express the selected basic support point by $P(x', y', 0)$ and let $\boldsymbol{V}_i = \boldsymbol{P}_i' - \boldsymbol{P}'$ (i=1,2,3), $\boldsymbol{V}_4 = \boldsymbol{V}_1$ and $\boldsymbol{W}_i = \boldsymbol{V}_i \times \boldsymbol{V}_{i+1}$ (i=1,2,3), $\boldsymbol{W}_4 = \boldsymbol{W}_1$. If $\boldsymbol{W}_i \cdot \boldsymbol{W}_{i+1} > 0$ (i=1,2,3), we can assure that P_s does locate in $\Omega(f)$. If there is a group of i and j meeting $\begin{cases} i,j \in (1,2,3) \\ i \neq j \end{cases}$ and $\begin{cases} V_i \times V_j = 0 \\ V_i \cdot V_j \leq 0 \end{cases}$, we can assure that P' does locate in $\Omega(s)$.

c. Calculate the ordinates of the cross point between the ray and the facet except its three sides. If P' locates in $\Omega(f)$, we could express any point in the ray created from P' by $\boldsymbol{R}(a) = \boldsymbol{P}' + a \cdot \boldsymbol{N}_{proj}$ and any point in the facet by $\boldsymbol{S}(b, c) = \boldsymbol{P}_1 + b \cdot (\boldsymbol{P}_2 - \boldsymbol{P}_1) + c \cdot (\boldsymbol{P}_3 - \boldsymbol{P}_1)$ where a, b and c are factors. So we can get the cross point $P(x, y, z)$ by solving $\boldsymbol{P} = \boldsymbol{R}(a) = \boldsymbol{S}(b, c)$. The result are $a = \frac{[(P_2 - P_1) \times (P_3 - P_1)] \cdot (P_1 - P')}{[(P_2 - P) \times (P_3 - P)] \cdot N_{proj}}$ and $\boldsymbol{P} = \boldsymbol{R}(a)$.

d. Calculate the ordinates of the cross point between the ray and the facet's three sides. If P' locates in $\Omega(s)$, we can get $P = P_i + \frac{\left|(P'-P_i)\times N_{proj}\right|}{\left|(P_j-P_i)\times N_{proj}\right|} \cdot (P_j - P_i)$.

e. Change to another basic support point if there exists any other basic points and go to step b.

As depicted in Fig. 12e, a physical part may be complex enough to need the support structures generating not only directly from the basement but also from the upward surfaces of the part. Therefore, after all facets are traversed, we should check whether there exist any unmarked facets and then find out all cross points between the unmarked facets and the rays out from the marked basic points. In fact, it's impossible that all the triangular facets of a physical part need to be marked to be supported.

After all unmarked facets are done, all of the cross points and the basic points must be classify by the support rays and then sorted from low to high. If there are still more than two points including the basic point in a support ray after deleting one of the highest points (P_{12}, P_{23}, P_{44}, P_{62}, P'_{71} in Fig. 12e), delete the coincident points according:

a. Find the two triangular facets in which located a pair of coincident points.

b. Calculate the cosines of the angles between the unit vector opposite the building direction and the normal vectors of the two facets.

c. If the product of those two cosines is negative, delete these two coincident points (P_{32}, P'_{32}, P_{51}, P'_{51} in Fig. 12e). Otherwise, delete one of them (P'_{11}, P'_{41} in Fig. 12e).

After that, if there are some points coinciding with the basic point in a support ray, delete all of them including the basic point (P_3, P_{31}, P_4, P_{41} in Fig. 12e). Then if the number of the points in this support ray is odd, we need to delete the highest point (P'_{23} in Fig. 12e) because it must locate in an unmarked facet. Finally, a single cross-shaped support piece in STL format can be created by a segment ending at a point pair consisting of every two points from low to high in one support ray (Fig. 12c). The width and the length of every single cross-shaped support piece are both set to be equal to the distance of every two adjacent basic support points. Therefore, all the single support pieces can be connected together to construct a block support which is same as that used in the foregoing experiments and also widely used in SLM (Fig. 12d).

3.3 Case study

In order to determine the effectivity of the proposed method, three typical parts (Table 4), namely blower impeller, ball and four-way valve, are used to be analyzed from the reduction in the number of the triangle facets needing supports and the volume of the supports. All of them are converted into STL format and positioned as shown in Table 4 wherein the red line is opposite to the recoating direction, i.e. direction of x-axis, and the green line is vertical to x, i.e. direction of y-axis. Their support structures are generated based on a same layout of basic support points where the distance between every two adjacent basic points in x-axis or y-axis is 0.5 mm as the value of f in Fig. 2b. All the supports are generated uprightly, i.e. $\boldsymbol{N}_{proj}$ = (0, 0, 1). Therefore, regardless of the actual thickness of the support pieces, the volume of every single cross-shaped support piece could be worked out by doubling the product of 0.5 mm and the distance of the two endpoints creating this single piece. Then the total volume of each parts' support structure can be obtained.

Table 4 Comparison of the supports generated by different methods.

alt-text: Table 4

Model	Total number of triangle facets	Target	Conventional	Proposed	Reduction (%)
1	70,476	Number of facets needing supports	9150	5537	39.5
		Volume of supports (mm²)	4232	1972	53.4
2	46,224	Number of facets needing supports	7992	7026	12.1
		Volume of supports (mm²)	3834	2446	36.2
3	29,354	Number of facets needing supports	3661	3227	11.9
		Volume of supports (mm²)	58,250	49,220	15.5

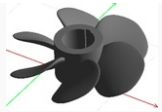 alt-text: Image 1	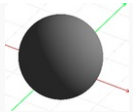 alt-text: Image 2	 alt-text: Image 3
1. blower impeller	2. ball	3. four-way valve

Two simple C++ programs were written out respectively based on the method proposed above and a conventional method. The conventional method determines whether ~~a~~ triangle facets need supports by a constant polar angle threshold. According to the aforementioned experimental results, the value of γ_{lim} varies with α from 24° to 32°. Therefore, in the conventional method, γ_{lim} must be assumed as a constant value of 32°. In this case, γ_s in Equation (6) is set to 0° and the support structures generated by these programs are showed in Fig. 13.

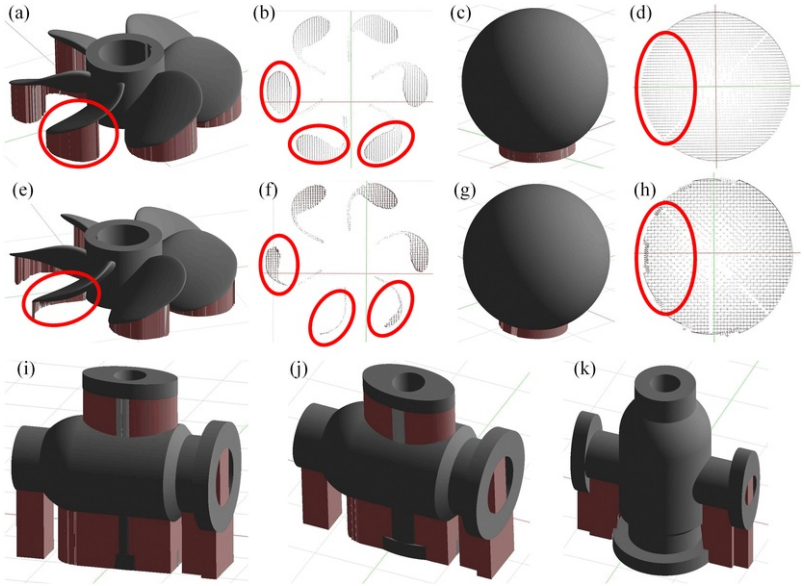

Fig. 13 Support structures generated by different methods: (a)(c)(i) by conventional method; (e)(g)(j) by proposed method; (b)(d)(f)(h) projections of supports in (a)(c)(e)(g); (k) by changing the orientation.

alt-text: Fig. 13

As listed in Table 4, comparing with the conventional method, both the number of the triangle facets needing supports and the volume of supports have a marked fall and shrank by 21.2% and 35% respectively using the slimmed-support generation method. For example, the support structure, highlighted by red in Fig. 13e and generated by the slimmed-support generation method, is much slimmer than that by the conventional method (Fig. 13a). Meantime, the projections of the support structures in the horizontal plane as depicted in Fig. 12b and Fig. 12f also illustrates that the volume of the support structures is reduced by the slimmed-support generation method. Although the number of the triangle facets needing supports is only cut down by 12.1%, the volume of the whole supports of the ball decreases largely by 36.2% because of the increase of the height of support piece away from the center. The projection of its support (Fig. 13h) is no longer in a circle (Fig. 13d). The number of the triangle facets needing supports and the volume of the supports of the four-way valve are cut down by ≥~~more than ten~~10 ~~percent~~%, although which can't been illustrated clearly by Fig. 13i and ~~Fig. 13~~j. If a 3D part contains many inclined surfaces whose polar angles are of 24° to 32°, this slimmed-support generation method will work much better.

Fig. 14 shows the practical formations of the blower impeller with three different support structures. The used powder material was also Ti-6Al-4V. The model could be completed well by both the conventional method according to a constant γ_{lim} of 32° and the proposed method while it failed to be built by the conventional method according to a constant γ_{lim} of 24° because of the failure circled in red (Fig. 14c).

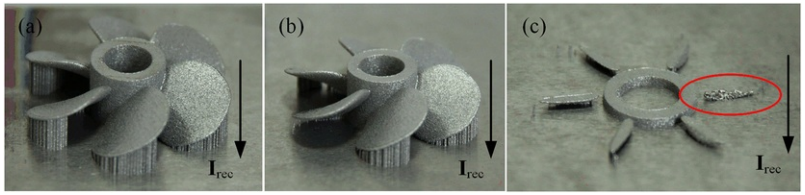

Fig. 14 Practical formations of the blower impeller with the support structures generated by: (a) the conventional method based on a constant γ_{lim} of 32°; (b) the proposed method; (c) the conventional method based on a constant γ_{lim} of 24°.

alt-text: Fig. 14

In addition, this slimmed-support generation method can be used to coordinate with other optimization methods of support slimming such as selecting the optimal build orientation of part [28, 38, 39]. Changing a part's orientation to reduce the support volume may increase the build height and consequently the manufacturing time. In the data available to some authors [40, 41], it is not clear that there is a significant correlation between build height and manufacturing time according to their multi-objective optimizations. Thus, from the factors considered by most researchers, the optimization of support volume remains one of the most critical factors for improving the efficiency of metallic additive layer manufacturing. Build orientation is a crucial parameter since it will affect the volume of support structures required [38]. For an instance, if the four-way valve was built in the orientation of Fig. 13k, the number of the triangle facets needing supports will be cut down to 1330 and the volume of the supports will be reduced to 23,907 mm^2. That is to say, the reductions of those two optimization targets will respectively reach 63.7% and 59%. In multi-axis additive manufacturing, the adaptation of the building direction is a key step as well in building parts without support structures [42]. For the in-plane anisotropy under a certain setting of process parameters it was found by Hitzler L. [43], that only the linear elastic properties and the breaking elongation were affected, whereas the other material properties such as relative density, surface hardness and tensile strength remained stable. On the other hand, if considering the anisotropy of the manufacturability of inclined surfaces, we will have more freedom in the design of 3D parts that can be built without supports relative to selecting a constant polar angle threshold.

~~4.~~4 Conclusions

In this research, a feasible method of support slimming was presented. Firstly, a series of experiments for exploring the thresholds of polar angles at different positions relative to the recoating direction of powders were conducted and the effect of powder recoating by scraper on the building of polar angles was analyzed. Then, a generation algorithm of reduced support structures was proposed based on the varying polar angle thresholds. In addition, three typical cases were applied to demonstrate the usefulness of this method. The obtained conclusions are as follows:

- **a.** The warpage of the specimen with small polar angle built at α=0° is suppressed by the scraper during the recoating process while that of the specimen built at α=180° is promoted by the scraper. The morphologies of their sharp corners have a significant distinction;
- **b.** The thresholds of the polar angles have a difference at different positions of α due to the distinction of the contact length between the scraper and the warpages;
- **c.** An effective slimmed-support generation method can be presented according the upper difference and it has been used to slim the support structures of three models by 35% in average. One of the models was practiced to further demonstrate the effectiveness of this proposed method;
- **d.** This method can be used to coordinate with other optimization methods of support slimming such as selecting the optimal build orientation of part to further optimize support structures.

Author ~~C~~contribution

Kaifei Zhang, David Z. Zhang conceived and designed the experiments;

Kaifei Zhang and Guang Fu performed the experiments;

Kaifei Zhang and Zhongfa Mao analyzed the data;

Kaifei Zhang and Chao Liu presented and verified the algorithm;

Kaifei Zhang wrote and revised the paper.

Acknowledgement

This work was supported by the National High-tech Research and Development Program of China (863 Program: 2015AA042501).

References

[1] J.J. Lewandowski and M. Seifi, Metal Additive Manufacturing: A Review of Mechanical Properties, *Annu. Rev. Mater. Res.* **46** (1), 2016, 151–186.

[2] F. Abe, K. Osakada, M. Shiomi, K. Uematsu and M. Matsumoto, The manufacturing of hard tools from metallic powders by selective laser melting, *J. Mater. Process. Technol.* **111** (1–3), 2001, 210–213.

[3] Z. Mao, D.Z. Zhang, P. Wei and K. Zhang, Manufacturing Feasibility and Forming Properties of Cu-4Sn in Selective Laser Melting, *Materials* **10** (4), 2017, 333.

[4] T. DebRoy, H.L. Wei, J.S. Zuback, T. Mukherjee, J.W. Elmer, J.O. Milewski, et al., Additive manufacturing of metallic components – Process, structure and properties, *Prog. Mater. Sci.* **92**, 2018, 112–224.

[5] H. Fayazfar, M. Salarian, A. Rogalsky, D. Sarker, P. Russo, V. Paserin, et al., A critical review of powder-based additive manufacturing of ferrous alloys: Process parameters, microstructure and mechanical properties, *Mater. Des.* **144**, 2018, 98–128.

[6] K. Abd-Elghany and D.L. Bourell, Property evaluation of 304L stainless steel fabricated by selective laser melting, *Rapid Prototyp. J.* **18** (5), 2012, 420–428.

[7] F. Calignano, Design optimization of supports for overhanging structures in aluminum and titanium alloys by selective laser melting, *Mater. Des.* **64**, 2014, 203–213.

[8] P. Singh and D. Dutta, Multi-Direction Slicing for Layered Manufacturing, *J. Comput. Inf. Sci. Eng.* **1** (2), 2001, 129–142.

[9] Y. Yang, J.Y.H. Fuh, T.L. Han and Y.S. Wong, Minimizing staircase errors in the orthogonal layered manufacturing system, *IEEE Trans. Autom. Sci. Eng.* **2** (3), 2005, 276–284.

[10] M. Matsumoto, M. Shiomi, K. Osakada and F. Abe, Finite element analysis of single layer forming on metallic powder bed in rapid prototyping by selective laser processing, *Int. J. Mach. Tool Manu.* *Int J Mach Tool Manu* **42** (1), 2002, 61–67.

[11] S. Mohanty and J. Hattel, Cellular Scanning Strategy for Selective Laser Melting: Capturing Thermal Trends with a Low-fidelity, Pseudo-Analytical Model, *Math. Probl. Eng.* **2014**, 2014, 1–14.

[12] H. Chen, D. Gu, J. Xiong and M. Xia, Improving additive manufacturing processability of hard-to-process overhanging structure by selective laser melting, *J. Mater. Process. Technol.* **250**, 2017, 99–108.

[13] D. Buchbinder, W. Meiners, N. Pirch, K. Wissenbach and J. Schrage, Investigation on reducing distortion by preheating during manufacture of aluminum components using selective laser melting, *J. Laser Appl.* **26** (1), 2014, 012004.

[14] V.E. Beal, P. Erasenthiran, N. Hopkinson, P. Dickens and C.H. Ahrens, The effect of scanning strategy on laser fusion of functionally graded H13/Cu materials, *Int. J. Adv. Manuf. Technol.* **30** (9–10), 2006, 844–852.

[15] L. Hitzler, J. Hirsch, B. Heine, M. Merkel, W. Hall and A. Ochsner, On the anisotropic mechanical properties of selective laser-melted stainless steel, *Materials* **10** (10), 2017.

[16] Z. Li, D.Z. Zhang, P. Dong and I. Kucukkoc, A lightweight and support-free design method for selective laser melting, *Int. J. Adv. Manuf. Technol.* **90** (9–12), 2016, 2943–2953.

[17] M. Leary, L. Merli, F. Torti, M. Mazur and M. Brandt, Optimal topology for additive manufacture: A method for enabling additive manufacture of support-free optimal structures, *Mater. Des.* **63**, 2014, 678–690.

[18] X. Guo, J. Zhou, W. Zhang, Z. Du, C. Liu and Y. Liu, Self-supporting structure design in additive manufacturing through explicit topology optimization, *Comput. Methods Appl. Mech. Engrg.* *Comput. Methods Appl. Mech. Eng.* **323**, 2017, 27–63.

[19] J.-P. Järvinen, V. Matilainen, X. Li, H. Piili, A. Salminen, I. Mäkelä, et al., Characterization of Effect of Support Structures in Laser Additive Manufacturing of Stainless Steel, *Phys. Procedia.* *Phys. Procedia* **56**, 2014, 72–81.

[20] G. Strano, L. Hao, R.M. Everson and K.E. Evans, A new approach to the design and optimisation of support structures in additive manufacturing, *Int. J. Adv. Manuf. Technol.* **66** (9–12), 2012, 1247–1254.

[21] J. Vanek, J.A.G. Galicia and B. Benes, Clever Support: Efficient Support Structure Generation for Digital Fabrication, *Comput. Graphics Forum* **33** (5), 2014, 117–125.

[22] M.X. Gan and C.H. Wong, Practical support structures for selective laser melting, *J. Mater. Process. Technol.* **238**, 2016, 474–484.

[23] R. Vaidya and S. Anand, Optimum support structure generation for additive manufacturing using unit cell structures and support removal constraint, *Procedia Manuf.* **5**, 2016, 1043–1059.

[24] K.A. Mumtaz, P. Vora and N. Hopkinson, A method to eliminate anchors/supports from directly laser melted metal powder bed processes, In: *Solid Freeform Fabr. Symp. Proc,* 2011.

[25] J. Jhabvala, E. Boillat, C. André and R. Glardon, An innovative method to build support structures with a pulsed laser in the selective laser melting process, *Int. J. Adv. Manuf. Technol.* **59** (1–4), 2011, 137–142.

[26] T.A. Krol, M.F. Zaeh and C. Seidel, Optimization of supports in metal-based additive manufacturing by means of finite element models, *Int. J. Robust Nonlinear Control* **25** (17), 2012, 3349–3366.

[27] Y.-H. Kuo, C.-C. Cheng, Y.-S. Lin and C.-H. San, Support structure design in additive manufacturing based on topology optimization, *Struct. Multidiscip. Optim.* **57** (1), 2017, 183–195.

[28] H.D. Morgan, J.A. Cherry, S. Jonnalagadda, D. Ewing and J. Sienz, Part orientation optimisation for the additive layer manufacture of metal components, *Int. J. Adv. Manuf. Technol.* **86** (5–8), 2016, 1679–1687.

[29] D.T. Pham and C. Ji, A study of recoating in stereolithography, *Proc. Inst. Mech. Eng. C J. Mech. Eng. Sci.* **217** (1), 2005, 105–117.

[30] B. Cheng and K. Chou, Geometric consideration of support structures in part overhang fabrications by electron beam additive manufacturing, *Comput. Aided Des.* **69**, 2015, 102–111.

[31] W. Di, Y. Yongqiang, S. Xubin and C. Yonghua, Study on energy input and its influences on single-track,multi-track, and multi-layer in SLM, *Int. J. Adv. Manuf. Technol.* **58** (9–12), 2011, 1189–1199.

[32] D. Wang, Y. Yang, Z. Yi and X. Su, Research on the fabricating quality optimization of the overhanging surface in SLM process, *Int. J. Adv. Manuf. Technol.* **65** (9–12), 2012, 1471–1484.

[33] N. Nadammal, A. Kromm, R. Saliwan-Neumann, L. Farahbod, C. Haberland and P.D. Portella, Influence of support configurations on the characteristics of selective laser-melted Inconel 718, *JOM.JOM* **70** (3), 2018, 343–348.

[34] P. Kulkarni, A. Marsan and D. Dutta, A review of process planning techniques in layered manufacturing, *Rapid Prototyp. J.* **6** (1), 2000, 18–35.

[35] X.P. Dong, The algorithm of pillar support generation for stereolithgraphy, *J. Huazhong Univ. Sci. Technolog. Med. Sci.* **32** (8), 2004, 16–18, (Nature Science Edition).

[36] P. Huang, C.C.L. Wang and Y. Chen, Algorithms for layered manufacturing in image space, In: *ASME Advances in Computers and Information in Engineering Research,* **1**, 2014, 377–410.

[37] L. Hitzler, M. Merkel, W. Hall and A. Öchsner, A review of metal fabricated with laser- and powder-bed based additive manufacturing techniques: process, nomenclature, materials, achievable properties, and its utilization in the medical sector, *Adv. Eng. Mater.* **20** (5), 2018, 1700658.

[38] P. Das, R. Chandran, R. Samant and S. Anand, Optimum part build orientation in additive manufacturing for minimizing part errors and support structures, *Procedia Manuf.* **1**, 2015, 343–354.

[39] K. Hu, S. Jin and C.C.L. Wang, Support slimming for single material based additive manufacturing, *Comput. Aided Des.* **65** (C), 2015, 1–10.

[40] N. Padhye and K. Deb, Multi-objective optimisation and multi-criteria decision making for FDM using evolutionary approaches, *Rapid Prototyp. J.* **17** (6), 2011, 458–478, (421).

[41] P.M. Pandey, K. Thrimurthulu and N.V. Reddy, Optimal part deposition orientation in FDM by using a multicriteria genetic algorithm, *Int. J. Prod. Res.* **42** (19), 2004, 4069–4089.

[42] D. Coupek, J. Friedrich, D. Battran and O. Riedel, Reduction of support structures and building time by optimized path planning algorithms in multi-axis additive manufacturing, *Procedia Cirp.* **67**, 2018, 221–226.

[43] L. Hitzler, J. Hirsch, J. Tomas, M. Merkel, W. Hall and A. Öchsner, In-plane anisotropy of selective laser-melted stainless steel: the importance of the rotation angle increment and the limitation window, *P. I. Mech. Eng. L-J. Mat.* 2018, (DOI:10.1177/1464420718757068).

Graphical abstract

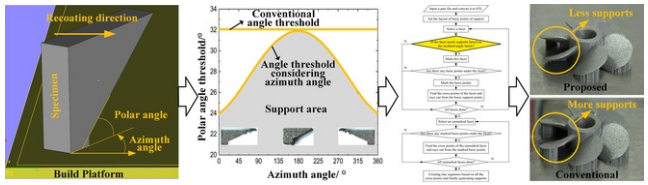

alt-text: Unlabelled Image

Highlights

- The threshold of polar angle varies with the azimuth angle due to the effect of recoating by scraper.
- A generation algorithm of slimmed support structures was presented based on the upper change.
- Several cases have verified the effectiveness of the proposed support-slimming method.
- This method can be used to coordinate with other optimization methods in selective laser melting.

Queries and Answers

Query:

Please check the layout of Table 3 if correct.

Answer: The layout of Table 3 is different from my original manuscript, which may makes the readers confused about the angles arranged in row and column. If possible,please modify it according to th attachment. In addition,the symbols highlighted by yellow background are originally symbols in red in my manuscript.Please modify them.Thank you.
Attachments: Table 3.docx

Query:

Please check the layout of Table 4 if correct.

Answer: Yes

Query:

Please confirm that given names and surnames have been identified correctly and are presented in the desired order, and please carefully verify the spelling of all authors' names.

Answer: Yes

Query:

The author names have been tagged as given names and surnames (surnames are highlighted in teal color). Please confirm if they have been identified correctly.

Answer: Yes

Query:

Would you consider changing the term “equitation” to “equation”? Please check, and amend as necessary.

Answer: Yes,please change "equitation" to "Eq.".

Query:

Have we correctly interpreted the following funding source(s) and country names you cited in your article: "Research and Development, United States".

Answer: No. Please don't modifiy the funding source in my manuscript. The National High-tech Research and Development Program of China (863 Program: 2015AA042501) is a program supported and managed by the ministry of science and technology of the People's Republic of China.

Query:

Please provide the volume number and page range for the bibliography in Ref. [43].

Answer: This is a conference paper and we have found out and read it carefully.Its page range is 1-15. However, the volume number of this paper cannot be found. We have provided its DOI instead.